Theoretical estimate of fivefold differential cross sections and spin asymmetry for K-shell $(e,3e)$ processes with transversely-spin-polarized relativistic electrons

R. Choubisa* and Munendra Jain

Department of Physics, Birla Institute of Technology and Science, Pilani 333031, India

(Received 11 April 2011; revised manuscript received 13 April 2012; published 1 August 2012)

Ab *initio* first-order Born calculations of the fivefold differential cross section (FDCS) and transverse spin asymmetry in FDCS for the K-shell double ionization of atoms by transversely polarized incident electron are reported. The FDCS and transverse spin asymmetry in FDCS are found to be sensitive to atomic number Z, ejection angle, and energy-sharing ratio of the ejected electrons. FDCS is decomposed into longitudinal and transverse contributions and their effects on the angular profile of FDCS such as shifting in the binary peak are reported. Hitherto, all $(e,3e)$ experiments have been performed in the nonrelativistic energy regime without consideration of spin polarization. We hope that the present calculation of FDCS and spin asymmetry in FDCS may induce quantum mechanically complete $(e,3e)$ experiments in the relativistic energy regime wherein spin-dependent interaction becomes prominent.

DOI: 10.1103/PhysRevA.86.022702 PACS number(s): 34.80.Dp, 34.80.Nz

I. INTRODUCTION

The transition of two electrons from the bound state to the continuum state by the impact of an incident electron on an atom [i.e., the $(e,3e)$ process] is a very important process for understanding the reaction mechanism, collision dynamics, and electron-electron correlation among the participating electrons in the process. In an $(e,3e)$ process, we detect all the outgoing electrons (scattered and ejected electrons) in coincidence after angular and energy analysis, and thus the coincidence cross section [here a fivefold differential cross section (FDCS)] contains the most detailed information about the electron impact double-ionization process of an atom. The first $(e,3e)$ measurement on an Ar atom was reported in 1989 [1] which stimulated more experimental and theoretical activities in the $(e,3e)$ field. The progress in the field was further accelerated after the first measurement on a He atom [2], particularly in the theory, because He is the simplest target for theoretical calculation of FDCS [2–5].

Hitherto, almost all theoretical and experimental activities in the $(e,3e)$ process have concentrated on the nonrelativistic energy regime wherein spin-dependent interaction plays no major role. We can understand the $(e,3e)$ process through a quantum mechanically complete experiment if we can include the spin of the participating electrons in our description. Various aspects related to spin-dependent interaction have been very well probed for the $(e,2e)$ field by studying triple differential cross section (TDCS) and spin asymmetry in various geometrical modes [6]. However, the $(e,3e)$ field is still unexplored in these aspects at relativistic energy. There is not even any theoretical estimation of FDCS and spin asymmetry in FDCS in the literature. The purpose of this paper is to look into this unexplored field by giving a theoretical estimation of FDCS and transverse spin asymmetry in FDCS in the relativistic energy regime for the K-shell double ionization of atoms and to explore the possibility of quantum mechanically complete $(e,3e)$ experiments in the relativistic energy regime, wherein spin-dependent interaction becomes prominent.

It is worth mentioning that Becher and Joulakian have described the Dirac plane wave for incident and scattered electrons for the $(e,3e)$ process [7]. They neglected spinors for bound and ejected electrons in the calculation of FDCS because they performed their calculation for a small Be atom with equal ejected-electron energies of 10 eV in their calculation. For these two cases, the relativistic effects are supposed to be smaller. Furthermore, they calculated the charge density term in their calculation of FDCS neglecting the current density term. In the present calculation, we calculate both charge and current density terms related to the incident-to-scattered electron transition. Furthermore, we also include relativistic effects for the bound K-shell electrons as well as those for the correlated ejected electrons in the continuum state because of their dominance in the present calculation. In addition, we report the transverse spin asymmetry in FDCS due to spin-polarized incident electrons.

II. THEORY

We develop our formalism with following assumptions:

(1) The incident electron emits a virtual photon at (x,t) along the direction of momentum transfer which is absorbed by the atom at (x',t') (see Fig. 1). The incident electron-atom interaction is of first order. Due to this interaction the incident electron is scattered by an angle θ_s from the incident electron direction.

(2) We also assume that the electromagnetic interaction, via a virtual photon interaction, emits the K-shell bound electrons into the continuum state. The fast and slow ejected electrons are ejected in the θ_1 and θ_2 direction, respectively, from the direction of the incident electron. All the electrons are in same plane (scattering plane).

(3) We describe incident and scattered electrons by a Dirac plane wave. We choose a Darwin-type wave function for the K-shell bound electrons [8].

(4) We describe the spatial part of the ejected electrons by approximated Brauner-Briggs-Klar (BBK) type wave functions [9] [the two Coulomb wave with Gamow factor (2CG) approach] with the Sommerfeld-Maue relativistic factor

*rjchoubisa@yahoo.co.in

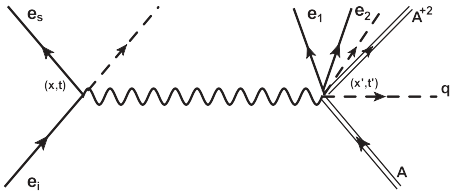

FIG. 1. Schematic diagram for $(e,3e)$ process on atom (A) by an incident electron (e_i). The electromagnetic interaction is mediated through a virtual photon along the momentum transfer direction q (θ_q, from the incident electron direction). The incident electron is scattered by θ_s from the direction of the incident electron (dash line), while fast and slow ejected electrons are ejected in θ_1 and θ_2 directions, respectively, from the direction of the incident electron. The spin of the incident electron is polarized perpendicular to the scattering plane.

[10,11]. For the singlet state of the ejected electrons, we keep the spatial part of the wave function symmetric and the spin part with asymmetric Dirac spinors. While for the triplet state, we keep the spatial part of the wave function asymmetric and the spinor part with the symmetric Dirac spinors.

Five-fold differential cross section for the $(e,3e)$ process can be evaluated by computing the following term:

$$\frac{d^5\sigma}{d\Omega_s d\Omega_1 d\Omega_2 dE_1 dE_2} = (2\pi)^4 \frac{k_s k_1 k_2}{k_i} \frac{E_i E_s E_1 E_2}{c^8} \bar{\sum_{\varepsilon_i,\varepsilon_{b_1},\varepsilon_{b_2}}} \sum_{\varepsilon_s,\varepsilon_1,\varepsilon_2} |\langle f|\hat{S}|i\rangle|^2, \quad (1)$$

where $\hat{S}$ is the S-matrix operator; i,s, 1, 2 and b_1,b_2 refer to the incoming, scattered, and fast and slow ejected electrons in the continuum state and those (i.e., 1 and 2) for the bound states, respectively. Here E_i, E_s, E_1, E_2 and k_i, k_s, k_1, k_2 are the on-shell total energies and momenta of the unbound particles, and ε are the spin projections with respect to the quantization axis, which we take along the momentum transfer direction.

FDCS here is insensitive to spin polarization because it is calculated as an average over initial-state spins and a sum over final-state spins. The main task here is to calculate the S-matrix element of the following form:

$$\langle f|\hat{S}|i\rangle = \frac{-1}{c} \int \mathbf{A}_\mu(r_1,r_2)\mathbf{J}^\mu(r_1,r_2) d^3r_1 d^3r_2, \quad (2)$$

where $\mathbf{A}_\mu(r_1,r_2)$ is a four-potential and can be expressed as

$$\mathbf{A}^\mu = \frac{4\pi}{(2\pi)^3} \frac{[u^\dagger(k_s,\varepsilon_s)\gamma^\circ\gamma^\mu u(k_i,\varepsilon_i)]}{\left[q^2 - \left(\frac{\Delta E}{c}\right)^2\right]} \{-Z + e^{i\mathbf{q}\cdot\mathbf{r}_1} + e^{i\mathbf{q}\cdot\mathbf{r}_2}\}. \quad (3)$$

Here $q = \mathbf{k}_i - \mathbf{k}_s$ is the momentum transfer, $\Delta E = E_i - E_s$, γ^μ are Dirac matrices, Z is the atomic number of the atom, and $u(k_i,\varepsilon_i)$ and $u(k_s,\varepsilon_s)$ are Dirac spinors of following form:

$$u(k,\uparrow) = \sqrt{\frac{E+c^2}{2E}} \begin{pmatrix} 1 \\ 0 \\ \frac{ck_z}{E+c^2} \\ \frac{c(k_x+ik_y)}{E+c^2} \end{pmatrix}, \quad (4a)$$

$$u(k,\downarrow) = \sqrt{\frac{E+c^2}{2E}} \begin{pmatrix} 0 \\ 1 \\ \frac{c(k_x-ik_y)}{E+c^2} \\ \frac{ck_z}{E+c^2} \end{pmatrix}. \quad (4b)$$

Here ($\uparrow$) and ($\downarrow$) attached to the spinors represent spin-up and spin-down polarization of the electrons. We describe the atomic transition four-current density for the electron transition from the K shell to the continuum state by $J^\mu(r_1,r_2)$ in the following form:

$$J^\mu(r_1,r_2) = c\psi_f^\dagger(r_1,r_2)\gamma^\circ\gamma^\mu\psi_i(r_1,r_2). \quad (5)$$

For the singlet state, $\psi_f(r_1,r_2)$ is the approximated symmetric BBK-type wave function [9] (2CG approach), multiplied by the asymmetric Dirac spinors for the ejected electrons. The wave function $\psi_f(r_1,r_2)$ has following form:

$$\psi_f(r_1,r_2) = \frac{C}{\sqrt{2}}\left[\phi_{k_1}(z_1,\mathbf{r}_1)\phi_{k_2}(z_2,\mathbf{r}_2) + \phi_{k_2}(z_2,\mathbf{r}_1)\phi_{k_1}(z_1,\mathbf{r}_2)\right] \times [u(k_1,\uparrow)u(k_2,\downarrow) - u(k_2,\downarrow)u(k_1,\uparrow)], \quad (6)$$

where $\phi_{k_j}(z_j,\mathbf{r_j})$ is the Coulomb wave function of the ejected electron j whose momentum is k_j. The repulsive Gamow factor C is given by

$$C = \exp\frac{-\pi}{k_{12}}\Gamma\left(1 - \frac{1}{k_{12}}\right), \quad (7)$$

where $k_{12} = \frac{|\mathbf{k}_1 - \mathbf{k}_2|}{2}$.

Alternately, there are three different forms of $\psi_f(r_1,r_2)$ for the triplet state of the ejected electrons (the spatial part is antisymmetric and the spinor part is symmetric):

$$\psi_f(r_1,r_2) = \frac{C}{\sqrt{2}}\left[\phi_{k_1}(z_1,\mathbf{r_1})\phi_{k_2}(z_2,\mathbf{r_2}) - \phi_{k_2}(z_2,\mathbf{r_1})\phi_{k_1}(z_1,\mathbf{r_2})\right] \times [u(k_1,\uparrow)u(k_2,\downarrow) + u(k_2,\downarrow)u(k_1,\uparrow)], \quad (8)$$

$$\psi_f(r_1,r_2) = C\left[\phi_{k_1}(z_1,\mathbf{r_1})\phi_{k_2}(z_2,\mathbf{r_2}) - \phi_{k_2}(z_2,\mathbf{r_1})\phi_{k_1}(z_1,\mathbf{r_2})\right] \times [u(k_1,\uparrow)u(k_2,\uparrow)], \quad (9)$$

$$\psi_f(r_1,r_2) = C\left[\phi_{k_1}(z_1,\mathbf{r_1})\phi_{k_2}(z_2,\mathbf{r_2}) - \phi_{k_2}(z_2,\mathbf{r_1})\phi_{k_1}(z_1,\mathbf{r_2})\right] \times [u(k_1,\downarrow)u(k_2,\downarrow)], \quad (10)$$

While $\psi_i(r_1,r_2)$ is an asymmetric Darwin wave function for K-shell electrons [12] with following form:

$$\psi_i(r_1,r_2) = Z'^3\left[a_{s_{b_1}}(\uparrow)a_{s_{b_2}}(\downarrow) - a_{s_{b_2}}(\downarrow)a_{s_{b_1}}(\uparrow)\right]e^{-Z'(r_1+r_2)}, \quad (11)$$

where $Z' = Z - 0.3$ is the effective nuclear charge and a_{s_b} is Darwin matrix of the following form (in atomic units):

$$a_{s_b}(\uparrow) = \begin{pmatrix} 1 \\ 0 \\ \frac{1}{2ic}\frac{\delta}{\delta z} \\ \frac{1}{2ic}\left(\frac{\delta}{\delta x} + i\frac{\delta}{\delta y}\right) \end{pmatrix}, \quad (12a)$$

$$a_{s_b}(\downarrow) = \begin{pmatrix} 0 \\ 1 \\ \frac{1}{2ic}\left(\frac{\delta}{\delta x} - i\frac{\delta}{\delta y}\right) \\ \frac{1}{2ic}\frac{\delta}{\delta z} \end{pmatrix}. \quad (12b)$$

In the calculation of matrix element $\langle f|\hat{S}|i\rangle$, we encounter the following types of spatial integrals:

$$I_1 = \int \phi_k^*(r) e^{i\mathbf{q}\cdot\mathbf{r}} e^{-Z'r} d^3r, \tag{13a}$$

$$I_2 = \int \phi_k^*(r) e^{i\mathbf{q}\cdot\mathbf{r}} \frac{\delta}{\delta x} e^{-Z'r} d^3r, \tag{13b}$$

$$I_3 = \int \phi_k^*(r) e^{i\mathbf{q}\cdot\mathbf{r}} \frac{\delta}{\delta y} e^{-Z'r} d^3r. \tag{13c}$$

$$I_4 = \int \phi_k^*(r) e^{i\mathbf{q}\cdot\mathbf{r}} \frac{\delta}{\delta z} e^{-Z'r} d^3r. \tag{13d}$$

In the calculation of FDCS, we consider all 64 possible combinations of spins of participating electrons. We separately calculate FDCS with spin-up [FDCS(↑)] and spin-down [FDCS(↓)] arrangements of incident electron. The unpolarized FDCS can be calculated as

$$(\text{FDCS})_{\text{unpolarized}} = \tfrac{1}{2}[\text{FDCS}(\uparrow) + \text{FDCS}(\downarrow)]. \tag{14}$$

We also calculate transverse spin-up and spin-down asymmetry A_T in FDCS as

$$A_T = \frac{\text{FDCS}(\uparrow) - \text{FDCS}(\downarrow)}{\text{FDCS}(\uparrow) + \text{FDCS}(\downarrow)}. \tag{15}$$

The spin asymmetry in K-shell ionization is caused by the spin-dependent forces, i.e., by Mott scattering (due to the spin orbit interaction of the continuum electrons moving with relativistic energies in the Coulomb field of the atomic nucleus). In the theory described here, the definition of Dirac spinor $u(k_i,s_i)$ for the incident electron, presumes that the mean spin direction of the electron is along $\mathbf{q}$. Taking the spin direction perpendicular to the collision plane, one has to rotate amplitude $\langle f|\hat{S}|i\rangle$ as suggested in Ref. [13]. For brevity, we are not discussing this derivation in detail and interested readers can follow Ref. [13] for further details.

III. RESULTS AND DISCUSSION

We have calculated FDCS and transverse spin asymmetry in FDCS for Ca, Zn, and Ag atoms. These targets were chosen to find the relativistic effects on FDCS and spin asymmetry with Z. Here we present FDCS (left panel) and transverse spin asymmetry in FDCS (right panel) in Fig. 2 as a function of the slow ejected electron angle θ_2, keeping θ_1 (the fast ejected electron angle) fixed along the momentum transfer direction. We keep the incident electron energy 340 and 88.2 keV for the ejected electrons. The energy of the scattered electron is chosen using energy conservation of the $(e,3e)$ process. We keep the angle of the scattered electron at a fixed angle -7° from the incident direction, and we change the energy-sharing ratio ($R = \frac{E_1}{E_2}$) between the two ejected electrons from 1 to 3.44. We have chosen a large energy for the ejected electrons to scale down multiple scattering of ejected electrons from the other bound electrons of the atom. Since we are considering atoms which have many electrons, particularly for the Ag atom, the chances of multiple scattering of ejected electrons with the bound electrons may increase at lower ejected electron energy.

We observed that the angular profile of FDCS is not symmetric about the momentum transfer direction even through the

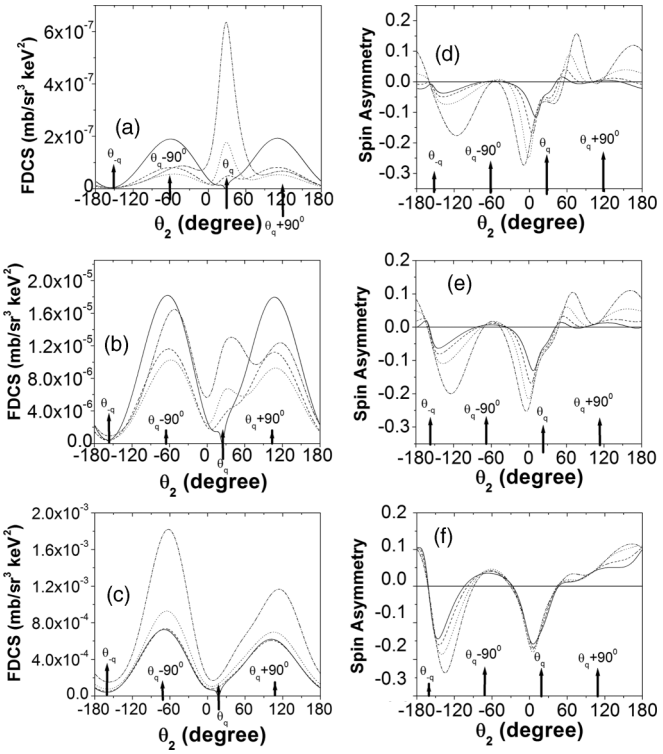

FIG. 2. FDCS (left panel) and spin asymmetry in FDCS (right panel) vs the angle of the slow ejected electron (θ_2) for (a), (d) Ca, (b), (e) Zn, and (c), (f) Ag targets. The kinematics used here is $E_i = 340$ keV, $\theta_s = -7^\circ$, $\theta_1 = \theta_q$ (momentum transfer direction). For solid curve: $E_1 = E_2 = 44.1$ keV; dashed curve: $E_1 = 52.1$ keV, $E_2 = 36.1$ keV; dotted curve: $E_1 = 60.1$ keV, $E_2 = 28.1$ keV; dash-dotted curve: $E_1 = 68.1$ keV, $E_2 = 28.1$ keV. The energy of the scattered electron for different targets can be found from the energy conservation. The arrows at $\theta_2 = \theta_q, \theta_2 = \theta_{-q}, \theta_q + 90^\circ$, and $\theta_q - 90^\circ$ refer to, respectively, the momentum transfer direction, opposite to the momentum transfer direction, and perpendicular to the momentum transfer direction.

present calculation is in the first order for the incident electron-projectile interaction. For most cases, we observed a two-peak structure located almost in the perpendicular direction to the momentum transfer axis [i.e., along $\theta_q + 90^\circ$ and $\theta_q - 90^\circ$ directions, see Figs. 2(a)–2(c)] and the distribution of FDCS for these two regions are not symmetric. Apart from these two peaks, we also observed a peak in the binary region ($\theta = \theta_q$) for lighter targets, like Ca and Zn targets [see Figs. 2(a) and 2(b)], for $R > 1$ (i.e., $E_1 > E_2$). It is well known that the symmetry in differential cross sections about the momentum transfer direction is found in the first-order Born calculations in the nonrelativistic $(e,2e)$ and $(e,3e)$ processes, and any deviation in the symmetry of differential cross sections, if observed, is due to second- or higher-order projectile-target interactions. However, symmetry breaking in TDCS (triple differential cross section) has also been observed for the $(e,2e)$ process in the relativistic energy regime, even for the first-order theory. Using the relativistic distorted-wave Born approximation (rDWBA) calculation, Ast *et al.* [14] attributed such type of shift to the effect of magnetic and retardation contributions of the electron-electron interaction and distortion effects in the incoming and outgoing channels of the $(e,2e)$

process. Bhullar and Sud [12] used the one-photon exchange approximation to demonstrate that the shift in the binary peak and formation of recoil peak in the $(e,2e)$ process occurs due to interference between the atomic transition charge density and current density contributions. Our first Born calculation also confirms such type of symmetry breaking in FDCS about the momentum transfer direction for the $(e,3e)$ process. It will be an interesting task to figure out the causes of such type of symmetry breaking in FDCS for the $(e,3e)$ processes.

The absolute cross section for these targets are found to be varied in range from μb/sr^3 keV^2 to 10^{-3} μb/sr^3 keV^2. The absolute TDCS reported for $(e,2e)$ process are found to be 2–200 mb/sr^2 keV for various atoms, which were mostly reported for 300 and 500 keV impact energies. If we compare the present results with the absolute data of TDCS reported in Ref. [6], it seems quite disappointing in terms of the feasibility of $(e,3e)$ experiments in the immediate future for the present kinematics. However, we will also find here another kinematics wherein the absolute FDCS can be increased significantly.

If we correlate angular profiles of FDCS with Z, we observe that the angular profile is not changing considerably for Ag atom with different R [see Fig. 2(c)]. However, for lower Z targets (i.e., for Ca and Zn targets), the angular profile of FDCS changes more rapidly with R [see Figs. 2(a) and 2(b)]. For the Ag atom though the peaks for different R are directed roughly in the same direction, their intensities (magnitude) do not vary sharply with R. We also observed that the two-peak structure for the Ag atom has one larger peak around $\theta_2 = -80^\circ$ and a relatively smaller peak around $\theta_2 = 105^\circ$ [see Fig. 2(c)]. These two peaks are roughly directed perpendicular to the momentum transfer direction (larger peak is in the $\theta_q - 90^\circ$ region; smaller peak, $\theta_q + 90^\circ$ region). For other targets, we have different features in the angular profile with R. For the Ca atom, the peak at $\theta_q \pm 90^\circ$ is found to be much smaller for larger R [dotted and dash-dotted curves in Fig. 2(a)]. However, we observed a dominant peak at $\theta = \theta_q$ for these R. The angular profile of Zn atom shows intermediate results of Ca and Ag atoms. Hence we observed that the perpendicular emission to momentum transfer direction for the slow ejected electron is more prominent for the Ag atom (heavy target); however, for the other lighter targets the slow electron prefers to get ejected in the momentum transfer direction. If we see the kinematics, we find that the perpendicular component of the momentum transfer along $\theta_q + 90^\circ$ and $\theta_q - 90^\circ$ direction is zero [i.e., $(\mathbf{k_i} - \mathbf{k_s})_{\text{perp}} = 0$]. As the fast ejected electron is fixed along the momentum transfer direction in the present calculation, the overall perpendicular component of $\mathbf{k_i} - \mathbf{k_s} - \mathbf{k_1}$ is zero, which results in $\mathbf{k_2} + \mathbf{q_r} = \mathbf{0}$ for the perpendicular direction (here $\mathbf{k_2}$ and $\mathbf{q_r}$ are the momenta of the slow ejected electron and nucleus, respectively). So the perpendicular emission of the ejected electron from the momentum transfer axis is through electron-nucleus scattering. Thus the angular profile at $\theta_q + 90^\circ$ and $\theta_q - 90^\circ$ should reflect the effect of the size of the nucleus. This is evident from the dominant peaks found at $\theta_q \pm 90^\circ$ for various R for the Ag atom, which has the heaviest nucleus in the present calculation. The dominance of peaks at $\theta_q + 90^\circ$ and $\theta_q - 90^\circ$ for the other two targets decreases systematically with decrement of Z, thus showing the signature of the effect of nucleus size on FDCS. For lighter atoms like Ca and Zn, we have a large variation in FDCS in two peaks with different R [see Figs. 2(a) and 2(b)]. However for the heaviest target, Ag, we do not observe considerable changes in FDCS with R. The heavier target makes the angular distribution of FDCS with R less sensitive; however, for light targets, the angular distribution of FDCS is more sensitive to R.

As far as the behavior of FDCS in the binary region is concerned (around the $\theta = \theta_q$ region), we have a node at $\theta = \theta_q$ for all the targets for $R = 1$ [see solid curves of Figs. 2(a)–2(c)] which is due to Coulomb repulsion between the ejected electrons which prevents them from ejecting in the same direction for $R = 1$ ($E_1 = E_2$). However, when R is increased from 1 ($E_1 > E_2$ case), the node at $\theta = \theta_q$ is filled. For the largest R ($R = 3.44$), the node around $\theta = \theta_q$ for $R = 1$ converts into a dominant peak for Ca and Zn atoms [see the dash-dot curve in Figs. 2(a) and 2(b)]. As R increases, the energy difference between the ejected electrons increases, which makes the Coulomb repulsion at $\theta = \theta_q$ weaker. This results in a larger possibility of the slower ejected electron to be ejected along $\theta = \theta_q$. For the Ca atom, the relative intensity of peaks at $\theta = \theta_q$ vary maximally with R [see Fig. 2(a)]. Formation of a peak at θ_q for higher R for Ca and Zn atoms can be inferred in terms of electron-electron correlation and the lesser role of nucleus played in the $(e,3e)$ process. The faster ejected electron detected at the momentum transfer direction carries a larger energy. The slower ejected electron will most probably be ejected along the momentum transfer after the shake-off process for lighter atoms. When both electrons are ejected along the momentum transfer, the recoil momentum carried by the ion will be minimum ($|\mathbf{q_r}| = |\mathbf{q} - \mathbf{k_1} - \mathbf{k_2}|$) and hence it will play the role of a spectator. This situation is naturally conducive for a lighter atom, which is evident from the angular profile of FDCS at $\theta = \theta_q$ for the Ca atom for larger R. For the heaviest atom in the present paper (i.e., Ag atom), the situation is not so conducive therefore we do not observe a peak at $\theta = \theta_q$ [see Fig. 2(c)].

For the similar kinematics and targets, we plot transverse spin asymmetry with angle θ_2 in the right panel of Fig. 2. If we correlate FDCS with spin asymmetry, we find significant spin asymmetry for smaller FDCS and lesser spin asymmetry for larger FDCS (see peaks in FDCS and corresponding asymmetry in Fig. 2). Our observation of finding large spin asymmetries in regions where the spin-inclusive FDCS is small is in agreement with the well-known effect from elastic electron atom scattering, where the correlation of large asymmetries with the minima of the differential cross section is interpreted as an indication of weak spin orbit coupling. It is worth mentioning that a similar type of observation was also found in the $(e,2e)$ process on atoms [6]. It seems that this feature is common to elastic scattering as well as ionization processes such as $(e,2e)$ and $(e,3e)$ reactions, even though all these processes are different in their nature.

We also observed that the spin asymmetry in the recoil region is largest for the Ag atom and smallest for the Ca atom [see Figs. 2(d) and 2(f) along the $\theta = \theta_{-q}$ direction]. The explanation of larger spin asymmetry for a heavier target in the $(e,2e)$ processes on atoms was given by Ast *et al.* [15]. The transverse spin asymmetry in the relativistic energy is caused by the spin orbital coupling of the continuum electrons with the Coulomb field of nucleus (Mott scattering). From the rest frame of the electron, the electron experiences the

magnetic field of the nucleus, and the magnetic moment of electron spin is coupled with the magnetic field of the nucleus. This coupling will produce asymmetry in FDCS for the spin-up and spin-down polarization of incident electrons. Prinz *et al*. [15] argued that the spin-orbital interaction should dominate for the recoil region because the nucleus takes a considerable part in the recoil region leading to a dominant contribution to asymmetry. Though the $(e,3e)$ process deals with the correlated motion of three outgoing electrons and hence substantively differs from $(e,2e)$ process, we have some common findings in these two processes. This is also evident from the spin asymmetry behavior in the region $\theta_q \pm 90^\circ$ where we found maximum asymmetry in Ag and minimum for the Ca atom. As discussed earlier, the dominant peak in this region is entirely from electron-nucleus scattering. Since the nucleus of Ag is heaviest, the spin asymmetry is largest here.

In the previous case, we facilitated very high energy for the ejected electrons ($E_1 + E_2 = 88.2$ keV) to reduce the chances of multiple scattering of ejected electrons with the other bound electrons of atom. However, this makes the magnitude of FDCS very small, which makes the feasibility of the $(e,3e)$ experiment difficult. As per our other calculation, we hope that the experiment can be made feasible if we reduce the energy available to the pair of ejected electrons (i.e., $E_1 + E_2$ small). Keeping this fact in mind, we further investigate FDCS with the scattering angle. We have already observed that the perpendicular emission to the momentum transfer is more probable for a Ag atom, so we keep $\theta_1 = \theta_q$ and $\theta_2 = \theta_q - 90^\circ$ and vary θ_s from 1° to 25° (here $\phi_s = 180^\circ$) for $R = 1$ ($E_1 = E_2 = 16.1$ keV). The angular profile of FDCS with θ_s is plotted in Fig. 3 for the Ag atom. The angular profile is found to be peaked around $\theta_s = 12^\circ$. The FDCS is increased significantly for this kinematics. It is found to be 4 mb/sr^3 keV^2 around $\theta_s = 12^\circ$, clearly a huge increment in FDCS from the previous kinematics. Keeping note of this, we further investigate FDCS as a function of θ_2 for Ca, Zn, and Ag atoms, $\theta_s = 12^\circ$ in Fig. 4.

We have chosen $E_1 = E_2 = 16.1$ keV so that FDCS can be inflated, meanwhile these energies should also fall within the relativistic energy regime, albeit sufficiently smaller than the earlier case we discussed. The chances of multiple scattering with other bound electrons as well as lesser dominance of the relativistic effect due to relatively smaller ejected electron energy may be debatable issues. However, our major concern here is the estimation of FDCS which is more practically feasible for the $(e,3e)$ experiment, therefore those issues can be neglected here.

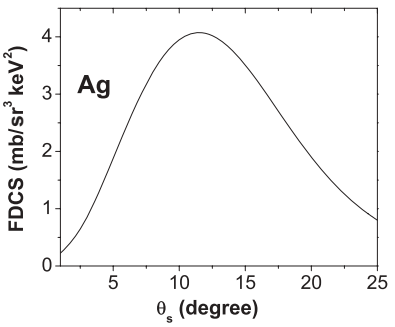

FIG. 3. FDCS vs the scattering angle θ_s ($\phi_s = 180^\circ$) for the Ag atom. The kinematics used here is $E_i = 340$ keV, $E_1 = E_2 = 16.1$ keV, and $\theta_1 = \theta_q$ and $\theta_2 = \theta_q - 90^\circ$.

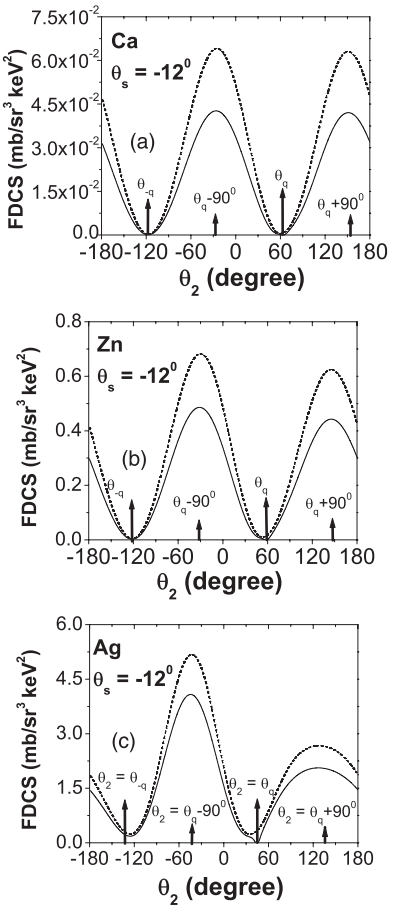

FIG. 4. FDCS vs angle θ_2 for $\theta_s = -12^\circ$ for (a) Ca, (b) Zn, and (c) Ag atoms with $\theta_1 = \theta_q$ (fixed angle). Solid and dotted curves represent FDCS for $R = 1$ and $R = 1.66$. The other kinematical variables are the same as Fig. 3.

We plot FDCS with θ_2, keeping θ_1 along the momentum transfer direction for the scattering angle $\theta_s = -12^\circ$ in Fig. 4 for Zn, Ca, and Ag atoms. The magnitude of FDCS has increased significantly. If we compare the angular profile of FDCS with Fig. 2 which pertains to different kinematics ($E_1 + E_2 = 88.2$ keV, $\theta_s = -7^\circ$), we found in the present kinematics that the perpendicular emission along $\theta_q \pm 90^\circ$ becomes more probable, even for the Ca atom, the lightest target in the present calculation. It is worth mentioning that in the earlier kinematics (refer to Fig. 2), the perpendicular emission along $\theta_q \pm 90^\circ$ was almost absent for the Ca atom [see Fig. 2(a)]. Furthermore, the degree of symmetry breaking of FDCS about $\mathbf{q}$ varies with Z. With the increment in Z, we observe that the angular profile becomes more asymmetric [see Fig. 4(c)]. In addition to this, the angular profiles of FDCS for different Z are found to be similar for $R = 1$ and $R = 1.66$ with the only difference found in their magnitude [see solid curve ($R = 1$) and dashed curve ($R = 1.66$) in Fig. 4].

Now, we calculate FDCS by calculating matrix elements separately for charge density and charge and current density

in a constant θ_{12} mode. We have twofold advantages here: (i) separation of FDCS in the aforesaid way will lead us to investigate the effect of magnetic interaction on FDCS and (ii) in the constant θ_{12} mode, the correlated motion of the ejected electrons can be modeled in terms of center of mass motion which may be useful to compare the $(e,3e)$ process with the $(e,2e)$ process [16,17]. The interaction between the incident electron and atom is mediated through a virtual photon which carries both longitudinal and transverse interactions [18]. The longitudinal interaction is along the momentum transfer direction and can be written as

$$S_{\rm fi}^{L} = \frac{-1}{c}\int (J_o a_o - J_q a_q)(-Z + e^{i\mathbf{q}\cdot\mathbf{r_1}} + e^{i\mathbf{q}\cdot\mathbf{r_2}})d^3r_1 d^3r_2, \tag{16}$$

where J_o and a_o are charge density and related Möller potential, respectively, while J_q and a_q are the components of current density and Möller potential along the momentum transfer direction, respectively. The transverse component can be written as

$$S_{\rm fi}^{T} = \frac{-1}{c}\int (J_T a_T)(-Z + e^{i\mathbf{q}\cdot\mathbf{r_1}} + e^{i\mathbf{q}\cdot\mathbf{r_2}})d^3r_1 d^3r_2, \tag{17}$$

where J_T and a_T are transverse components of four-current and Möller potential, respectively. We plot FDCS with $\theta = \frac{\theta_1+\theta_2}{2}$ in Fig. 5 for the Ag target (with $R = 1$). We keep other kinematical conditions the same as in Fig. 4. In the constant θ_{12} mode, we keep the mutual angle between the ejected electrons constant (here $\theta_{12} = 30^\circ$) and vary their angles (θ_1 and θ_2). We plot FDCS with the bisecting angle of mutual angle ($\theta = \frac{\theta_1+\theta_2}{2}$). For $R = 1$ (symmetrically ejected electrons), θ represents the direction of center of mass of the ejected electron ($\mathbf{k_c} = \mathbf{k_1} + \mathbf{k_2}$). If we consider the analogy between $(e,2e)$ and $(e,3e)$ processes, we can describe the $(e,3e)$ process in terms of a quasibinary collision between the incident electron and center of mass. The origin of *binary* and *recoil* peaks can be understood if we consider the center of mass momentum $\mathbf{k_c} = \mathbf{k_1} + \mathbf{k_2}$ which is in the direction of θ for case $|\mathbf{k_1}| = |\mathbf{k_2}|$. So the variation of FDCS with θ is equivalent to the variation of FDCS with the direction of the center of mass of the ejected electrons $\mathbf{k_c}$.

(i) When $\mathbf{k_c}$ is in the direction of $\mathbf{q}$ (here $\mathbf{q} = \mathbf{k_1} + \mathbf{k_2} + \mathbf{q_r} = \mathbf{k_c} + \mathbf{q_r}$), the recoil momentum ($\mathbf{q_r} = \mathbf{q} - \mathbf{k_c}$) is minimum and the momentum carried by the center of mass of the ejected electrons is maximum. This results in the formation of a *binary peak* in the direction of momentum transfer.

(ii) When $\mathbf{k_c}$ is in the direction opposite to the momentum transfer, the recoil momentum ($\mathbf{q_r} = \mathbf{q} + \mathbf{k_c}$) is maximum. The ion plays an active role here, resulting in a recoil peak at θ_{-q}.

When we consider FDCS due to the longitudinal contribution ($|S_{\rm fi}|^2$), we get a binary peak at θ_q (see dashed curve). Further, when we consider FDCS due to the transverse term (dotted curve), we observe a profound shift in the binary peak (around 30° shift from the $\theta = \theta_q$ direction) and small peaks at the $\theta_q \pm 90^\circ$ direction. Both contributions ($|S_{\rm fi}^L|^2 + |S_{\rm fi}^T|^2$), when added together, follow almost the same pattern as that for the transverse term. When we add the interference term of longitudinal and transverse interaction in $|S_{\rm fi}^L|^2 + |S_{\rm fi}^T|^2$ (i.e., FDCS $\cong |S_{\rm fi}^L + S_{\rm fi}^T|^2$), we observed that the interference term shifts the binary peak toward the forward direction (see solid curve) and also increases FDCS of the binary peak. In addition to this, the interference term reduces FDCS in the other regime.

Here, we have used two Coulomb waves for the ejected electrons with the Gamow factor in our calculation of FDCS. We calculated FDCS with and without the Gamow factor to investigate its effect on angular profile. We kept the same kinematics and geometry as we used in Fig. 4 and present the results for the Ag target. The results are plotted in Fig. 6. We observed that the Gamow factor makes an angular profile that is different only in a smaller angular range between the ejected electrons (i.e., the region in proximity to the other ejected electron direction, see the $\theta_1 = \theta_q$ arrow). However, for larger angles, we observed that the Gamow factor does not make any prominent differences in the angular profile. Further, the Gamow factor reduces the absolute cross section marginally (see solid and dotted curves in Fig. 6). It is worth mentioning that the nonrelativistic calculation reported with the Gamow factor usually destroys the normalization of TDCS for the $(e,2e)$ process (see, e.g., Whelan *et al.* [19] and Kheifets *et al.* [20]). The present relativistic calculation also destroys the normalization of FDCS for the $(e,3e)$ process, albeit marginally.

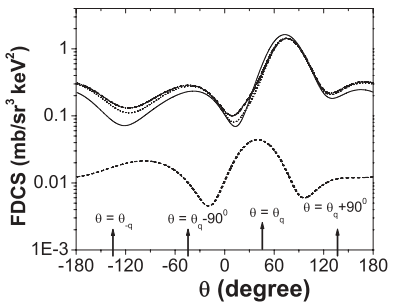

FIG. 5. FDCS in terms of longitudinal (L) $|S_{\rm fi}^L|^2$ and transverse (T) $|S_{\rm fi}^T|^2$, $|S_{\rm fi}^L|^2 + |S_{\rm fi}^T|^2$, and $|S_{\rm fi}^L + S_{\rm fi}^T|^2$ with θ for the Ag atom with equal energy-sharing ratio ($R = 1$) for constant mutual angle $\theta_{12} = 30^\circ$ for $E_1 = E_2 = 16.1$ keV, $\theta_s = 12^\circ$. Dash, dot, dash-dot, and solid curves represent FDCS due to $|S_{\rm fi}^L|^2$, $|S_{\rm fi}^T|^2$, $|S_{\rm fi}^L|^2 + |S_{\rm fi}^T|^2$, and $|S_{\rm fi}^L + S_{\rm fi}^T|^2$, respectively.

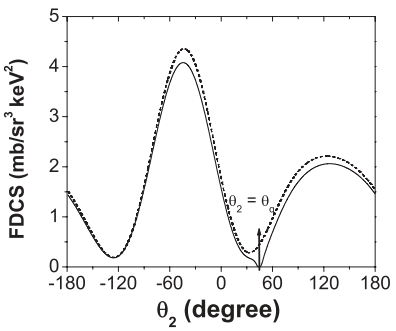

FIG. 6. FDCS with the Gamow factor (solid curve) and without the Gamow factor (dotted curve) as a function of θ_2 keeping θ_1 fixed along θ_q (see arrow at $\theta_1 = \theta_q$). The other kinematical variables are $E_i = 340$ keV, $E_1 = E_2 = 16.1$ keV, $\theta_s = -12^\circ$.

IV. CONCLUSION

In conclusion, we have reported FDCS and spin asymmetry in FDCS for Ca, Zn, and Ag atoms in a relativistic regime using the first-order Born approximation. We observed that FDCS is sensitive to atomic number Z, ejection angle, and energy-sharing ratio $\frac{E_1}{E_2}$ between the ejected electrons. We have found a shift in the binary peak in the constant θ_{12} mode. The effects of longitudinal and transverse interactions as well as their interference terms have been investigated in the constant θ_{12} mode. The incident electron spin polarization effects are investigated through transverse spin asymmetry and are found to be larger where FDCS is smaller. Such correlations between spin asymmetry and FDCS are also found to be common in well-established elastic scattering (Mott scattering) and single ionization [i.e., $(e,2e)$] processes.

Hitherto, all $(e,3e)$ experiments had been performed in nonrelativistic energy regime without consideration of spin polarization. Here, we have suggested a different type of $(e,3e)$ experiment in which we can include the spin of the participating electrons. We have also investigated the kinematical condition wherein the FDCS is larger. This may induce $(e,3e)$ experiments in near future for the suggested kinematics. This will definitely make our understanding of the $(e,3e)$ process much better in terms of the role of spin correlation of the participating electron in the complicated $(e,3e)$ process on atoms.

Here, we would like to stress that the present formulation has described Dirac spinors for the ejected electrons which totally depend upon the kinematical parameters and hence veiling the dynamical features of the $(e,3e)$ process. A better approximation would be choosing space-dependent Darwin matrices for the ejected electrons. This may explore hidden dynamical effects of spin interplay of the ejected electrons. In additional to this, it is worth mentioning that due to computational complexities of the problem, we did not include the exchange effect between the incident electron and scattered electron and their exchange effects with the other participating electrons in the $(e,3e)$ process. Perhaps a more complete picture will emerge about the reported FDCS and spin asymmetry after these incorporations. Since the $(e,3e)$ results in the relativistic energy regime have not been reported earlier, the reported results are naturally not conclusive and have to be confirmed with the other theoretical results. The reported data will be a step towards better understanding of the complicated $(e,3e)$ process on atoms in the relativistic energy regime.

ACKNOWLEDGMENTS

We are thankful to DST, New Delhi, for providing us Grant No. SR/FTP/PS-77/2007 under the Young Scientist Scheme. Authors are also thankful to the referee of the paper for his critical comments on the form of the ejected electron wave function, particularly about the triplet state transition of the ejected electrons.

[1] A. Lahmam-Bennani, C. Dupré, and A. Duguet, Phys. Rev. Lett. **63**, 1582 (1989).
[2] I. Taouil, A. Lahmam-Bennani, A. Duguet, and L. Avaldi, Phys. Rev. Lett. **81**, 4600 (1998).
[3] A. Lahmam-Bennani, A. Duguet, M. N. Gaboriaud, I. Taouil, M. Lecas, A. Kheifets, J. Berakdar, and C. D. Cappello, J. Phys. B **34**, 3073 (2001).
[4] R. Choubisa and K. K. Sud, J. Phys. B **41**, 208002 (2008).
[5] A. Dorn, A. Kheifets, C. D. Schröter, B. Najjari, C. Höhr, R. Moshammer, and J. Ullrich, Phys. Rev. Lett. **86**, 3755 (2001).
[6] W. Nakel and C. T. Whelan, Phys. Rep. **315**, 409 (1999).
[7] M. Becher and B. Joulakian, J. Phys. B **42**, 065206 (2009).
[8] D. M. Davidovic, B. L. Moiseiwitsch, and P. H. Norrington, J. Phys. B **11**, 847 (1978).
[9] M. Brauner, J. S. Briggs, and H. Klar, J. Phys. B **22**, 2265 (1989).
[10] A. Sommerfeld and A. Maue, Ann. Phys. **22**, 629 (1935).
[11] M. E. Rose, *Relativistic Electron Theory* (Wiley, New York, 1961).
[12] A. S. Bhullar and K. K. Sud, Indian J. Phys. B **73**, 299 (1999).
[13] D. H. Jakubassa-Amundsen, Phys. Rev. A **53**, 2359 (1996).
[14] H. Ast, S. Keller, R. M. Dreizler, C. T. Whelan, L. U. Ancarani, and H. R. J. Walters, J. Phys. B **29**, L585 (1996).
[15] H. T. Prinz, K. H. Besch, and W. Nakel, Phys. Rev. Lett. **74**, 243 (1995).
[16] R. Choubisa, G. Purohit, and K. K. Sud, J. Phys. B **36**, 1731 (2003).
[17] A. Lahmam-Bennani, A. Duguet, and S. Roussin, J. Phys. B **35**, L59 (2002).
[18] A. S. Bhullar, Ph.D. thesis, M.L.S. University, Udaipur, 2001.
[19] C. T. Whelan, R. J. Allan, J. Rasch, H. R. J. Walters, X. Zhang, J. Roder, K. Jung, and H. Ehrhardt, Phys. Rev. A **50**, 4394 (1994).
[20] A. S. Kheifets, A. Naja, E. M. S. Casagrande, and A. Lahmam-Bennani, J. Phys. B **41**, 145201 (2008).